Thermal Efficiency of Arc Welding Processes

The effect of welding parameters and process type on arc and melting efficiency is evaluated

BY J. N. DuPONT AND A. R. MARDER

ABSTRACT. A study was conducted on the arc and melting efficiency of the plasma arc, gas tungsten arc, gas metal arc, and submerged arc welding processes. The results of this work are extended to develop a quantitative method for estimating weld metal dilution in a companion paper. Arc efficiency was determined as a function of current for each process using A36 steel base metal. Melting efficiency was evaluated with variations in arc power and travel speed during deposition of austenitic stainless steel filler metal onto A36 steel substrates.

The arc efficiency did not vary significantly within a given process over the range of currents investigated. The consumable electrode processes exhibited the highest arc efficiency (0.84), followed by the gas tungsten arc (0.67) and plasma arc (0.47) processes. Resistive heating of the consumable GMAW electrode was calculated to account for a significant difference in arc efficiency between the gas metal arc and gas tungsten arc processes.

A semi-empirical relation was developed for the melting efficiency as a function of net arc power and travel speed, which described the experimental data well. An interaction was observed between the arc and melting efficiency. A low arc efficiency factor limits the power delivered to the substrate which, in turn, limits the maximum travel speed for a given set of conditions. High melting efficiency is favored by high arc powers and travel speeds. As a result, a low arc efficiency can limit the maximum obtainable melting efficiency.

J. N. DUPONT and A. R. MARDER are with the Department of Material Science and Engineering, Lehigh Univ., Bethlehem, Pa.

Introduction

The term thermal efficiency used in this work describes the welding process in two ways, namely arc efficiency and melting efficiency. Arc efficiency provides a quantitative measure of the fraction of total arc energy delivered to the substrate. The rate of energy generated by the arc is given simply by the product of current and arc voltage. The heat input, a more widely used quantity, is the ratio of arc power to travel speed and represents the quantity of energy generated by the arc per unit length of weld. The net arc power and heat input, those energy quantities actually delivered to the substrate, are used extensively in heat-flow models to predict the thermal cycles in the substrate which, in turn, control phase transformations and the associated mechanical properties. Use of the net energy delivered to the suhstrate requires knowledge of the arc efficiency. Therefore, it is important to know the arc efficiency of a welding process in order to accurately utilize heat-flow models. The arc efficiency must also be known in order to experimentally measure melting efficiency, the second efficiency factor.

KEY WORDS

Thermal Efficiency
Melting Efficiency
PAW
GTAW
GMAW
SAW
Weld Parameters
Arc Efficiency
Energy Transfer

It is well known that a relatively small portion of the net energy is actually used for melting. The ratio of energy used for melting to that which is delivered to the substrate defines the melting efficiency. The qualitative energy balance of the welding process that accounts for the arc and melting efficiencies is schematically represented in Fig. 1, which is modified from Niles and Jackson (Ref. 1). The majority of total energy from the process is provided by the welding arc, while a small portion is generated at the electrode. The energy generated by the arc and electrode is basically distributed in two ways; a portion is lost to the environment, and the remainder is transferred to the workpiece. The net energy delivered to the work piece is also basically distributed in two ways; a portion is used for melting of the fusion zone while the remainder is lost to the adjacent base metal outside of the fusion zone primarily by thermal conduction. The energy lost to the base metal outside the fusion zone contributes to the formation of the heat-affected zone (HAZ) and heating of the base metal outside the HAZ above the ambient temperature. The total energy balance can be expressed as

$$E_{arc+electrode} = E_{losses} + E_{fz} + E_{bm} \quad (1)$$

The left side of Equation 1 represents the total energy generated by the process. E_{losses} represents losses to the environment, which are quantified by the arc ef

ficiency factor. E_{fz} represents the energy used for melting of the fusion zone, and E_{bm} represents the energy lost to the surrounding base metal. The summation of E_{fz} and E_{bm} represents the total energy transferred to the work piece by the process. The arc efficiency, η_a, and the melting efficiency, η_m, are then given as

$$\eta_a = \frac{E_{fz} + E_{bm}}{E_{arc+electrode}} \quad (2)$$

$$\eta_m = \frac{E_{fz}}{E_{fz} + E_{bm}} \quad (3)$$

It should be noted that the definition of arc efficiency given by Equation 2 actually represents energy transferred to the base metal from both the arc and electrode. A true value of energy transferred only from the arc (and thus a true "arc" efficiency value) would require a voltage measurement from the electrode tip to the base metal, which is difficult and impractical. It is more common to measure the combined electrode and arc voltages and base the arc efficiency on these values. Meaningful comparisons among processes can thus be made if the voltage measurements are kept consistent in this manner from process to process. The term thermal transfer efficiency may be more descriptive in this regard. However, the term arc efficiency is more commonly used and will be utilized here by the definition given in Equation 2.

The arc efficiency is only slightly affected by the welding parameters for a given process. It is generally viewed that nonconsumable electrode processes exhibit a slightly lower arc efficiency than the consumable electrode processes (Refs. 2, 3). This difference among the two types of processes has, in a qualitative manner, been attributed to the transfer of electrode energy to the substrate, which occurs with the consumable electrode processes. However, this claim has not been verified in a quantitative sense. The melting efficiency depends strongly on the arc power and travel speed (Refs. 4–6) until a theoretical maximum value of 0.48 is achieved for two-dimensional heat-flow conditions. After this point, adjustments in processing parameters provide no further increase in the melting efficiency. Since the primary objective of a welding process is to provide energy to the base metal for melting of the fusion zone, it becomes an important task to maximize the melting efficiency by careful adjustment of the welding parameters. Parameters that lead to an optimized melting efficiency will reduce the size of the heat-affected zone, minimize wasted process energy, and reduce distortion.

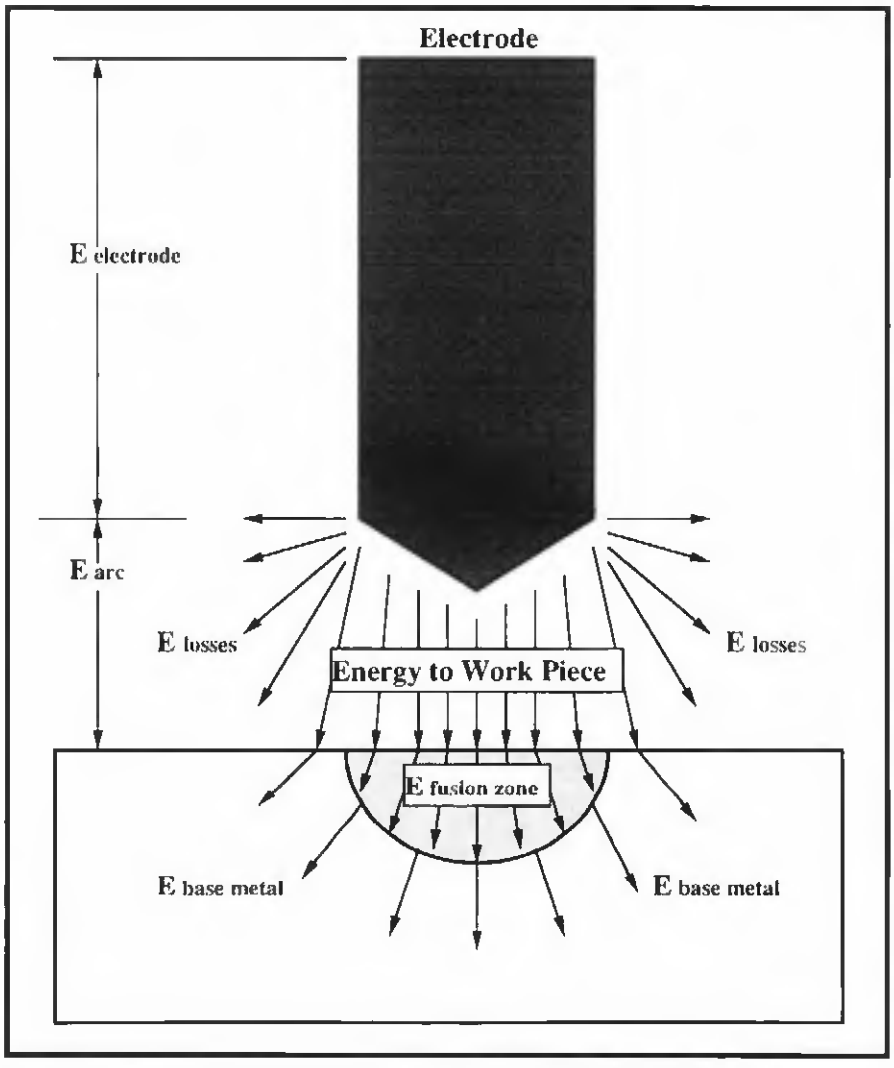

Fig. 1 — Schematic illustration showing the energy distribution in the welding process.

(Of course, applications exist where the parameters must be optimized based upon other priorities, such as the welding of steels where cold cracking can be reduced or eliminated by slower travel speeds to reduce the cooling rate.) Several relations between arc power, travel speed and melting efficiency have been reported (Refs. 4–6), which provide an opportunity to predict optimum welding parameters in terms of melting efficiency. In addition to melting efficiency optimization, a correlation between melting efficiency and the welding parameters, together with knowledge of the arc efficiency, can be used to predict the energy distribution of the process entirely from the welding parameters. Such knowledge is also useful for predicting optimized welding parameters for surfacing applications from simple energy balance relations, an approach that is discussed in a companion paper (Ref. 7).

The main objectives of the present study are: 1) measure the arc efficiencies of consumable and nonconsumable electrode processes and estimate the contribution of the consumable electrode energy to the arc efficiency factor, and 2) develop a correlation between the melting efficiency and welding parameters. The results of this work will be useful for predicting the thermal efficiency of the welding process from the welding parameters. In particular, the thermal efficiency of the plasma arc welding (PAW), gas tungsten arc welding (GTAW), gas metal arc welding (GMAW), and submerged arc welding (SAW) processes during deposition of austenitic stainless steel onto carbon steel was investigated.

Experimental Procedure

Welding Processes

A fully automated welding system designed specifically for research was used for all the experiments in this study. A 500-A constant current/constant voltage

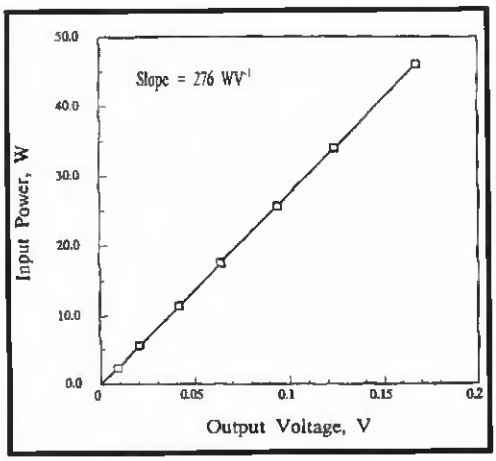

Fig. 2 — Calibration plot for the arc welding calorimeter. The slope of the plot defines the calibration constant.

power source was used for each process. A separate plasma console unit was used for control of the pilot arc, plasma gas, and shielding gas for the PAW process. Motion of the individual torches was provided by an automated travel carriage. The power source, travel carriage, and all auxiliary equipment are controlled by a Texas Instruments/Siemens programmable control unit.

The PAW and GTAW processes were conducted using direct current electrode negative (DCEN) polarity with a 4-mm (0.16-in.) diameter, 2%-thoriated tungsten electrode and argon shielding gas. The PAW torch was designed specifically for surfacing applications. A large constricting nozzle was used, which contained two ports for delivery of powder filler metal into the liquid pool. When used, the powder filler metal was fluidized in an argon gas and delivered to the nozzle ports by a calibrated screw feeder. Argon was used as the plasma gas.

The GMAW and SAW processes were conducted using direct current electrode positive (DCEP) polarity with a 1.14-mm (0.045-in.) diameter 308 austenitic stainless steel welding wire. Argon shielding gas was used for the GMAW process. The voltage was measured between the torch and substrate with a programmable volt meter. For all the processes, the measured voltage represents the sum of voltage drops across the electrode and arc. Current was measured by a calibrated shunt placed in series with the current carrying cable.

Arc Efficiency Measurements

Arc efficiency measurements were conducted using a Seebeck arc welding calorimeter. This apparatus, first described for arc efficiency measurements by Giedt, *et al.* (Ref. 8), works on the gradient layer principle where a voltage output is produced that is proportional to the heat flux through the calorimeter walls. When a welded sample is placed in the calorimeter, the integrated voltage-time curve produced as the substrate cools to equilibrium, multiplied by a calibration constant, yields the total quantity of energy transferred to the workpiece by the welding process. The voltage signal from the calorimeter was measured as a function of time by a personal computer with a data acquisition system.

The system was calibrated by placing a calibration heater inside the calorimeter, inducing a known voltage across the heater, and measuring the resultant heater current. At steady state, the heater input power divided by the output signal of the calorimeter yields the calibration constant of the calorimeter. Figure 2 shows calibration results for a range of input power and displays the linear response of the calorimeter. The slope in Fig. 2 defines the calibration constant and was measured at 276 WV^{-1}. This value was within 1% of the calibration constant specified by the manufacturer.

To use the calorimeter for arc efficiency measurements, samples were welded and then quickly placed in the calorimeter. The resultant voltage signal was recorded as a function of time by the data acquisition system as the samples cooled to room temperature and the voltage signal was reduced to zero. The total heat content of the welded sample was obtained by integrating the voltage-time plot and multiplying the integrated voltage signal by the calibration constant. The integration was performed using the personal computer and internal software. Weld times were kept below 10 s to minimize heat losses prior to placing the sample in the calorimeter. Transfer times to the calorimeter after welding were held below 3 s. For the arc efficiency measurements, a 100-mm square by 25-mm thick (4-in. square by 1-in. thick) A36 steel substrate was used. Heat losses during welding and transfer are caused by evaporation, radiation, and convection. Evaporation and radiation from the liquid pool during welding of iron have been estimated to be on the order of 30 and 10 W, respectively (Ref. 9). Losses due to convection, P_c, are given by

$$P_c = (T-T_o)^{1.25}\, h\, A_{bm} \qquad (4)$$

where T is the elevated surface temperature, T_o is the ambient temperature, h is the convection coefficient, and A_{bm} is the surface area of the base metal. The surface temperature will obviously vary with position, but an effective value of 700 K can be used, which should yield an upper bound value of heat losses due to convection. With T_o = 300 K, A_{bm} = 0.03 m^2, and h = 1.6 $Wm^{-2}K^{-1.25}$ (Ref. 10), the rate of heat loss due to convection is approximately 85 W. Thus, the total rate of heat loss during welding is approximately 125 W, which is typically on the order of 1% of the total arc power. Therefore, heat losses during welding and transfer to the calorimeter can basically be neglected. This general conclusion has been reported in other work as well (Refs. 6,11,12).

After determining the total heat content of the weld sample, the arc efficiency is calculated by

$$\eta_a = \frac{E_{cal}}{VIt} \qquad (5)$$

where V is the voltage, I is the current, t is the welding time, and E_{cal} is the energy content obtained from the calorimeter measurement. Experimental measurements have shown that arc efficiency varies only slightly with changes in processing parameters (Refs.6,11,13). Therefore, arc efficiency was measured only as a function of current. With the GMAW and SAW processes, current is increased by increasing the welding wire feed rate, so current variations also correspond to variations in welding wire feed rate. The nominal range of primary parameters used for the arc efficiency measurements are listed in Table 1. The contact tube-to-work distance of the GMAW process was adjusted for each current and voltage setting to produce a nominal electrode extension of 12 mm (0.48 in.). The electrode extension of the SAW process was not controlled due to the inability to observe the arc and electrode. Instead, the contact tube-to-work distance was held constant at 15 mm (0.6 in.). Fused flux from the SAW process was removed before the samples were inserted into the calorimeter. For the GTAW process, the electrode-to-work distance was held constant at 6 mm (0.23 in.). The stand-off distance of the PAW process was held constant at 15 mm (0.6 in.) with a plasma gas flow rate of 1 L/min.

Melting Efficiency Measurements

Once the arc efficiency was characterized for each process, the melting efficiency was investigated by depositing additional welds under the range of parameters listed in Table 2, holding all

other variables constant at the values cited above for the arc efficiency measurements. Note that these ranges are essentially identical to the ranges listed in Table 1 used for the arc efficiency measurements. As previously noted, the thermal efficiency measurements of this work were generated for use in parameter optimization of surfacing applications, and the parameters selected for study were chosen based on their importance in surfacing. To simulate a typical surfacing procedure, Type 308 austenitic stainless steel was deposited onto A36 carbon steel for each process. The steel substrates were 305 mm square by 6.4 mm thick (12 in. square x 0.25 in. thick) and each weld was approximately 254 mm (10 in.) in length. The PAW process utilized filler metal in powder form as described above. A cold wire feeder supplied a 1.14-mm (0.045-in.) diameter wire to the weld pool for the GTAW process. The GMAW and SAW processes also used a 1.14-mm (0.045-in.) diameter electrode. The ranges listed for each process were determined by preliminary weld trials. The lower limit to travel speed for a given arc power was governed by the formation of excessively wide and deeply penetrating welds. The upper limit of travel speed was established for a given arc power when the process could no longer adequately melt the substrate and filler metal. Thus, the values listed in Table 2 represent a wide range of operable parameters for each process under the conditions described.

After welding, each sample was cross-sectioned using an abrasive cut-off wheel, polished to a 1-μm finish using silicon carbide paper, and etched in a 2% Nital solution. The individual cross-sectional areas of the melted substrate and deposited filler metal were then measured using a quantitative image-analysis system. The cross-sectional area terms were multiplied by the total weld length to determine the individual volumes of the melted substrate and deposited filler metal. Melting efficiency was then determined by

$$\eta_m = \frac{E_{fm} v_{fm} + E_s v_s}{\eta_a V I t} \quad (6)$$

Where $E = \int C_p(T)dT + \Delta H_f$ (C_p - specific heat, ΔH_f - latent heat of fusion) represents the energy required to raise the filler metal (E_{fm}) and substrate (E_s) to the melting point and supply the latent heat of fusion, v_{fm} is volume of deposited filler metal, and v_s is the volume of melted substrate. The pertinent values of E are E_{fm} = 8.7 J/mm³ for 308 austenitic stainless steel (Ref. 14) and E_s = 10.5 J/mm³ for carbon steel (Ref. 15). The value used here for 308 austenitic stainless steel was actually reported for 304 and 304L austenitic stainless steel since no data could be found for 308. However, it has been shown (Ref. 16) that the slight variations in chemical compositions among these grades of stainless steels have a negligible effect on the specific heat.

Results and Discussion

Arc Efficiency

Figure 3 shows the arc efficiency for each welding process as a function of welding current. A clear distinction in the ability of each process to transfer energy to the workpiece is evident. The data also show there is very little variation in arc efficiency over the current ranges investigated. The consumable electrode processes (GMAW and SAW) exhibit an average arc efficiency of 0.84 ± 0.04. The GTAW process has an average arc efficiency of 0.67 ± 0.05, and the PAW process displays an average arc efficiency of 0.47 ± 0.03. These values are in good agreement with other arc efficiencies reported in the literature for these processes. For example, Smartt, *et al.* (Ref. 11), measured the arc efficiency of the GTAW process. For the range of current that was similar to the present work, the arc efficiency was approximately 0.70. This measurement was reported for a 304 stainless steel anode.

The anode material can have an effect on arc efficiency since approximately 56% of the energy transfer is attributed to the anode work function (Ref. 9). However, the arc efficiencies for 304 and 316 stainless steel and A36 steel were essentially equivalent, suggesting that the work functions of these materials are similar. (This also demonstrates that the use of an A36 steel anode for the GTAW and PAW processes and the use of an austenitic stainless steel anode with the GMAW and SAW processes, as done here, should have no contribution to the differences in arc efficiencies displayed in Fig. 3.) Watkins, *et al.* (Ref. 13), measured the arc efficiency of the GMAW process on carbon steel using filler metal feed rates similar to the present work and reported a nominal value of 0.85. Based on the similarities of the GMAW and SAW processes, it is not surprising to find that the arc efficiencies for these processes are essentially identical. The low arc efficiency of the PAW process is somewhat surprising since this process is

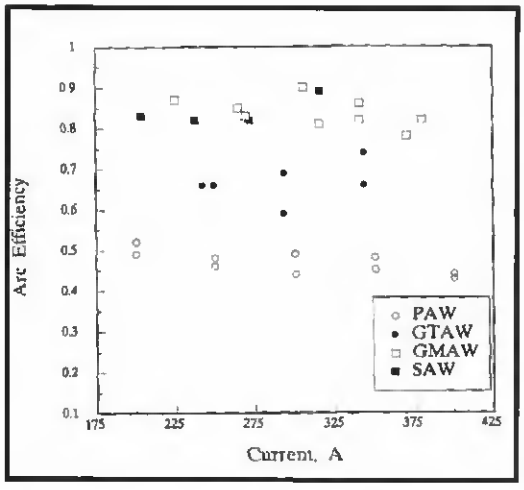

Fig. 3 — Arc efficiency for the PAW, GTAW, GMAW and SAW processes as a function of welding current.

Table 1 — Experimental Matrix of Processing Parameter Ranges Used in Arc Efficiency Experiments

Process	Current (A)	Voltage (V)	Travel Speed (mm/s)	Filler Metal Feed Rate mm³/s
PAW	200–400	24–32	3	None
GTAW	250–350	15–16	7	None
GMAW	230–375	27–35	15	120–235
SAW	200–320	34–37	15	120–240

Table 2 — Experimental Matrix of Processing Parameter Ranges Used in Melting Efficiency Experiments

Process	Current (A)	Voltage (V)	Travel Speed (mm/s)	Filler Metal Feed Rate mm³/s
PAW	250–400	25–32	2–4	8–120
GTAW	250–400	15–16	6–10	20–130
GMAW	230–400	27–36	6–26	120–245
SAW	200–330	34–37	6–26	120–245

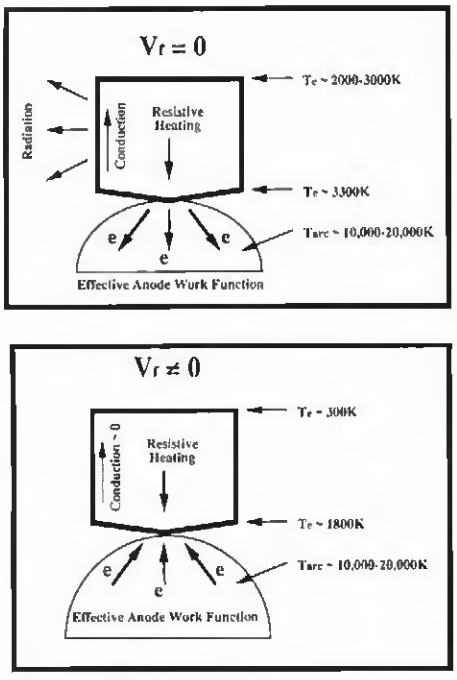

Fig. 4 — Heat flow conditions. A — Stationary GTAW electrode ; B — moving GMAW electrode .

similar to the GTAW process. This will be discussed in more detail later.

It has been suggested (Refs. 2, 3) that the high arc efficiency of the consumable electrode processes (compared to the nonconsumable electrode processes) is caused by transfer of energy from the moving electrode to the substrate, a process which does not occur with stationary electrodes. This phenomenon can be rationalized in a more quantitative way by considering the energy balance equations for the electrode in the GTAW and GMAW processes. Considering a small control volume, Kou and Tsai derived an energy balance equation (in terms of energy per unit volume) for the GTAW stationary electrode as (Ref. 17)

$$\frac{\partial}{\partial x}\left(k\frac{\partial T_e}{\partial x}\right)+I^2\left(\frac{\rho}{A_{cs}^2}\right)-\left(\frac{C}{A_{cs}}\right)\sigma\varepsilon\left(T_e^4-T_{noz}^4\right)=0 \qquad (7)$$

Where k is thermal conductivity, x is position along the electrode length, p is resistivity, σ is the Stefan-Boltzmann constant, ε is emissivity, T_e and T_{noz} are the temperature of the electrode and inside wall of the torch nozzle, respectively, A_{cs} is the cross-sectional area of the electrode, and C is the electrode circumference. Equation 7 applies from the point on the electrode collet where current enters the electrode to the electrode tip. This condition is shown schematically in Fig. 4A. The first term represents heat flow due to conduction from the high-temperature arc through the tip of the tungsten electrode towards the cooler collet. The second term represents heat generated due to resistive heating and the last term represents heat losses due to radiation. Convective losses are considered negligible (Ref. 17). Kou used this energy balance to determine the temperature distribution within the tungsten electrode and found good agreement with experimentally measured temperature profiles, indicating Equation 7 adequately describes the heat flow condition of the stationary electrode. Therefore, heating of the electrode by thermal conduction from the arc and resistive heating is balanced by radiation losses and thermal conduction to the electrode collet. The important point to note here is that no energy within the electrode due to thermal conduction and resistive heating is transferred to the substrate. In fact, a slight amount of heat is lost from the high-temperature arc by conduction through the electrode.

The heat flow in a consumable electrode (shown schematically in Fig. 4B) with volumetric filler metal feed rate, V_{fm}, has been considered by Ref. 18. Two major terms, resistive heating of the electrode and electron absorption onto the electrode tip, provide energy for melting and superheating of the electrode. Energy due to resistive heating is generally not sufficient to raise the electrode to the melting temperature. Thus, in the solid portion of the electrode, the balance of power terms yields

$$I^2R=\left(\int_{T_0}^{T_s}C_{ps}\,dT\right)\cdot V_{fm} \qquad (8)$$

where $T_s < T_m$ (T_m = the melting temperature), R is the effective resistance of the wire given by $(\rho(T)L/A_{cs})$, where $\rho(T)$ is the temperature-dependent resistivity, which varies along the length L due to the variation in temperature with L, and C_{ps} is the specific heat of the solid. Equation 8 applies from the point where current enters the electrode at the contact tube up to the point behind the liquid/solid interface where $T = T_s$. Energy from electron absorption onto the electrode tip provides the additional energy required for melting and superheating of the electrode to T_{dr}

$$I\phi=\left(\int_{T_s}^{T_m}C_{ps}dT+\Delta H_f+\int_{T_m}^{T_{dr}}C_{pl}dT\right)\cdot V_{fm} \qquad (9)$$

where ϕ is the effective anode work function, ΔH_f is the latent heat of fusion, and C_{pl} is the specific heat of the liquid. Radiation and convection losses can be considered negligible (Ref. 18). A conduction term should also be considered to account for heat flow from the liquid drop to the solid. However, this term has been shown to contribute significantly to heating of the solid electrode only at distances less than 0.5 mm from the solid-liquid interface (Ref. 18). Considering this portion of the electrode is small compared to the total electrode extension (12 mm in this work), the thermal conduction term can be neglected with little error. This can be verified by a simplified calculation. The temperature difference within the 0.5 mm at the solid electrode tip where thermal conduction plays a role can be approximated as = 300°C (572°F) (Ref. 18). Assuming, for the sake of this simplified estimation, the temperature distribution is linear, then power from thermal conduction can be approximated by $P = A_{cs}k\,(\Delta T/x)$. Using an upper bound value of k for pure iron of 0.06 W/(mm°C) at 1300°C (2372°F) (Ref. 22), ΔT = 300°C, x = 0.5 mm, and Acs = 1 mm² for a 1.14-mm diameter electrode, P ≈ 36 W. The calculations below will show that power from resistive heating and electron absorption are on the order of 1000 W and 3000 W, respectively, for the current ranges considered in this work. Thus, as already indicated (Ref. 18), the conduction term is negligible.

From the considerations above, it is evident that any resistive heating in the GTAW electrode is balanced by radiation losses and thermal conduction to the electrode collet, while with the GMAW process, resistive heating of the electrode is transferred to the substrate when the filler metal is deposited as weld metal. Thus, the resistive term in Equation 8 represents a major difference in power transfer between the GMAW and GTAW processes. Since it is generally accepted that resistive heating is not sufficient to heat the filler metal to its melting temperature and then melt it (Ref. 18), this difference in power, ΔP, between the processes can be expressed as

$$\Delta P=I^2R=\left(\int_{T_n}^{T_s}C_{ps}dT\right)V_{fm} \qquad (10)$$

where $T_s < T_m$.

An analytical solution to the effective resistance of the consumable electrode wire has been developed by Wasznik and Van Den Heuvel and is given by Ref. 18.

$$R=\frac{\lambda L}{A_{cs}}-\frac{\beta V_{fm}\rho_d}{I^2} \qquad (11)$$

where λ is the resistivity for T > 1300 K

and is equal to 1.3×10^{-3} Ωmm for austenitic stainless steel and $\beta = 1.7 \times 10^{2}$ J/g for austenitic stainless steel (Ref. 18). ρ_d is the electrode density. This relation is quite useful as it does not require knowledge of the temperature variation within the electrode since it evaluates the effective resistance as an integrated quantity. Calculation of the effective R for the range of currents, electrode extension and filler metal feed rates used here with the GMAW process yielded a value which was essentially constant at 0.014 Ω. Therefore, the difference in power transfer, ΔP, between the GTAW and GMAW processes from resistive heating can be expressed simply as

$$\Delta P = 0.014 \cdot I^2 \qquad (12)$$

By comparing this value with the total power transferred to the substrate, $P_s = \eta_a VI$, with $\eta_a = 0.84$ for the GMAW process, the expected differences in arc efficiency from the resistive power term between the GMAW and GTAW processes can be evaluated and compared with the measured differences. The total substrate power can be expressed exclusively as a function of current by noting that, in the range of current and voltage used here, $V = a + bI$. This behavior is shown in Fig. 5 where the data can be fit to the linear regression equation

$$V = 12.9 + 0.06 \cdot I \qquad (13)$$

Therefore,

$$Ps = \eta_a \cdot I \cdot (12.9 + 0.06 \cdot I) = 10.84 \cdot I + 0.05 \cdot I^2 \qquad (14)$$

Equations 12 and 14 are plotted as a function of current in Fig. 6 to reveal the fraction of total power supplied to the substrate by the electrode, which is not available with the GTAW process. ΔP ranges from 14 to 18% of P_s. If this fraction of power is subtracted from the total power delivered to the substrate, the arc efficiency of 0.84 for the GMAW process is reduced to 0.69 to 0.72. This value is close to the measured arc efficiency range of 0.67 ± 0.03 for GTAW, indicating that the major difference in arc efficiency between the GMAW and GTAW processes can be attributed to power delivered by resistive heating of the filler metal. (Based on the comparable arc efficiencies of the GMAW and SAW processes, a similar argument probably holds for the SAW process as well. However, the calculations could not be made because L was unknown.)

It is also useful to consider the fraction of total power supplied by the super-heated molten drops, P_{drop}, as given by the sum of the resistive power term in Equation 8 and the electron absorption term in Equation 9. The effective anode work function, ϕ, can be taken as 6V (Ref. 18). Using ϕ = 6 V and R = 0.014 Ω, P_{drop} can then be written as

$$P_{drop} = 6 \cdot I + 0.014 \cdot I^2 \qquad (15)$$

Equations 14 and 15 are plotted as a function of current in Fig. 7 where it can be seen that the super-heated drops account for 38 to 42% of the total power supplied to the substrate. This calculated value is in good agreement of the work conducted by Watkins, *et al.* (Ref. 13), where P_{drop} was measured and found to account for approximately 38 to 46% of the total power delivered to the substrate. Lastly, since $(\Delta P/P_s)$ and (P_{drop}/P_s) do not vary significantly with current, the arc efficiency is expected to remain fairly constant with variations in the welding current. This is shown in Fig. 8 where $(\Delta P/P_s)$ and (P_{drop}/P_s) are plotted as a function of current and found to vary only slightly over the range of current evaluated here. Again, this behavior is reflected in the experimental data of Fig. 3.

The arc efficiency of the PAW process used in this work is very low (0.48). It has been estimated (Ref. 19) that the PAW arc efficiency should exceed that of the GTAW process due to increased energy transfer by convection (due to higher gas flow rates) and radiation (due to higher arc temperatures). However, the analysis did not include heat losses from the arc to the nozzle which surrounds the recessed tungsten electrode and a portion of the arc. With the PAW torch used in these experiments, a massive metallic nozzle surrounds the recessed tungsten electrode and a portion of the arc. The nozzle acts as a heat sink, effectively absorbing energy from the arc before it can be transferred to the substrate. An extreme indication of the

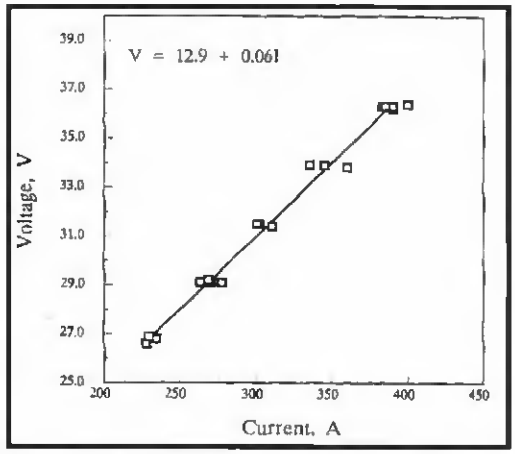

Fig. 5 — Voltage plotted as a function of current for the GMAW process showing the linear relation between voltage and current in the range of parameters used.

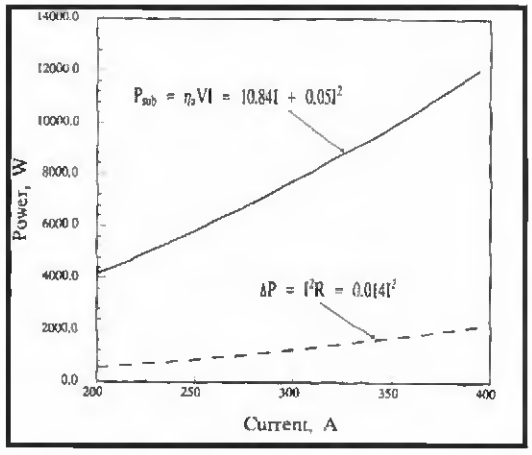

Fig. 6 — Plot of $\Delta P = 0.014 \cdot I^2$ and $P_s = 10.84 \cdot I + 0.05 \cdot I^2$ as a function of current showing the portion of total power supplied to the workpiece by resistive heating of the electrode in the GMAW process.

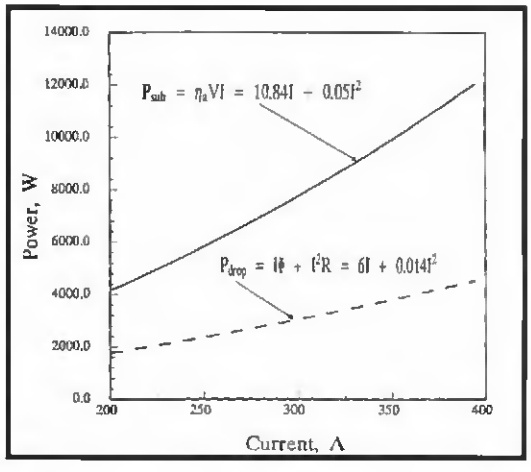

Fig. 7 — Plot of $P_{drop} = 6 \cdot I + 0.014 \cdot I^2$ and $P_s = 10.84 \cdot I + 0.05 \cdot I^2$ as a function of current showing the portion of total power supplied to the work piece by the superheated drops.

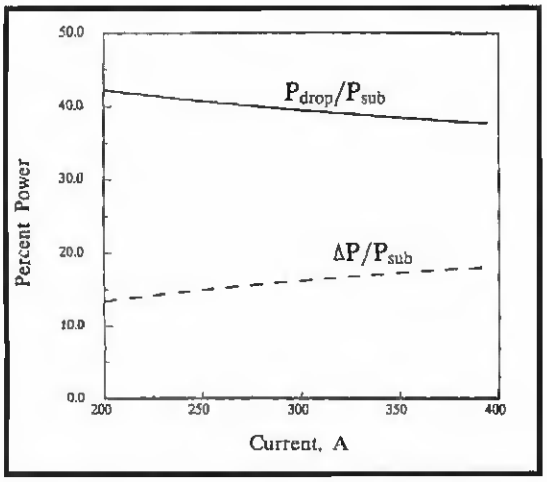

Fig. 8 — Plot of $\Delta P/P_s$ and P_{drop}/P_s as a function of current showing the contribution of each term to the total power supplied to workpiece.

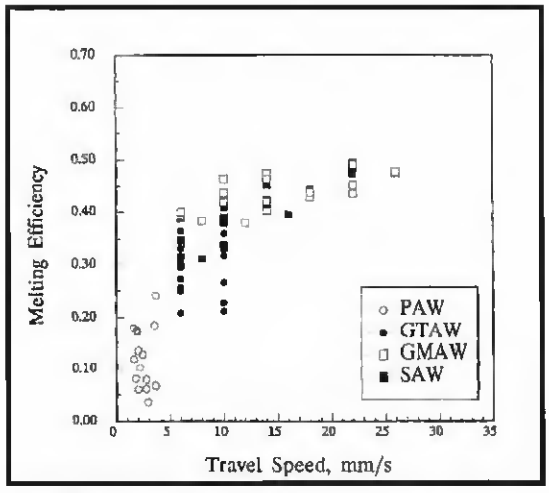

Fig. 9 — Melting efficiency of all the processes as a function of travel speed.

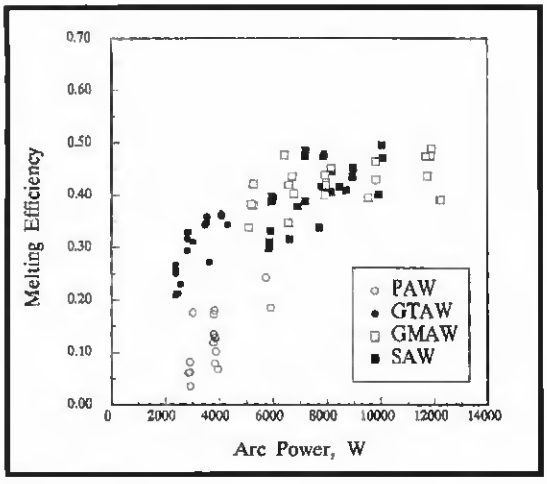

Fig. 10 — Melting efficiency of all the processes as a function of net arc power.

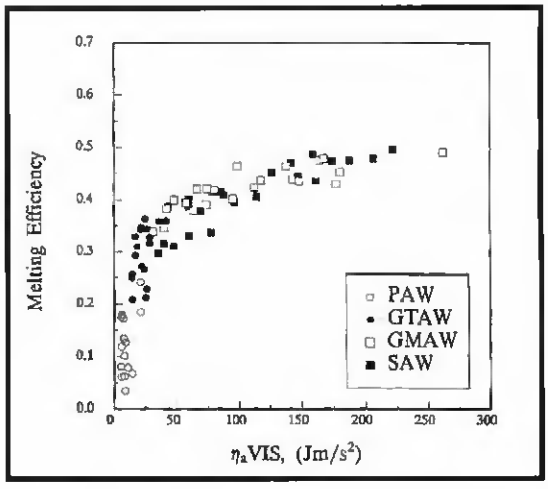

Fig. 11 — Melting efficiency of all the processes as a function of the product of net arc power and travel speed, $\eta_a VIS$.

heat losses to the nozzle was revealed in one high-amperage run where a section of the nozzle began to melt. A similar phenomenon has been reported by Fuerschbach and Knorovsky (Ref. 6). In fact, their arc efficiency values were ≈0.50 when heat losses to the nozzle were high. This value is within the range of 0.47 ± 0.03 measured here. In the work of Fuerschbach and Knorovsky, the arc efficiency was increased when the nozzle size was changed and heat losses were reduced. However, with the torch design used in these experiments, a massive nozzle is required for powder delivery into the arc and the arc, efficiency remains low as a result. Therefore, a large part of the radiation and convective heat transfer, which has been considered to be a significant contribution to energy transfer in the PAW process, is absorbed by the torch nozzle and promotes a substantial reduction in arc efficiency.

Melting Efficiency

Wells (Ref. 4) showed that melting efficiency should depend on the dimensionless ratio (α/Sd) (α is the base metal thermal diffusivity, S is the welding speed, d is the weld width) and proposed the analytical expression of Equation 16 for melting efficiency as a function of travel speed (for two-dimensional heat flow).

$$\eta_m = \frac{1}{\frac{8\alpha}{5Sd} + 2} \qquad (16)$$

This relation accounts for the rapid increase in melting efficiency with travel speed and the saturation of η_m to a value of 0.48 at high travel speeds when the ratio of thermal diffusivity to travel speed is low, which has been observed experimentally (Refs. 4, 6, 20). However, attempts to correlate the melting efficiency exclusively to travel speed have generally been unsuccessful. Figure 9 shows the melting efficiency as a function of travel speed for all the processes evaluated. Although the expected trend of increasing melting efficiency with increasing travel speed is ob-

served, along with the saturation of melting efficiency to ≈0.48, there is considerable scatter in the data.

Figure 10 shows the melting efficiency as a function of net arc power delivered to the substrate where it is observed that increases in the net arc power also increase the melting efficiency. However, as with travel speed, the scatter in the data is significant. Okada (Ref. 5) has shown a correlation between melting efficiency and the product of arc power and travel speed, suggesting a synergistic relation between these two parameters. Figure 11 shows the melting efficiency of all the processes as a function of η_aVIS, the product of arc power and travel speed. The arc power is multiplied by the arc efficiency so that the true magnitude of power reaching the substrate is considered. The results show that each process occupies a rather discrete section of the plot due to differences in arc efficiency and maximum achievable travel speeds among the process. However, the data all lie on one curve and are continuous from process to process, showing that melting efficiency is indeed controlled by the product of arc power and travel speed, independent of the process considered. This result can be rationalized by considering the competition of localized energy transport to the work piece by the moving heat source and transport away from the locally heated area to the surrounding cooler substrate by thermal conduction.

The power delivered to the substrate is generally consumed in one of two ways. A portion of the power is used to provide the enthalpy change required for localized melting and super-heating of the liquid weld pool. The remaining power is transported away from the locally heated area to the surrounding substrate mainly by thermal conduction. The melting efficiency is determined by the ratio of power used for melting to the total power delivered to the substrate. A competition exists between the instantaneous power (η_aVI) delivered locally to the substrate by the heat source moving at speed (S) and the transport of power away from the local region by thermal conduction. Therefore, if the rate of energy transport (*i.e.*, power) to the locally heated region is increased, less time is effectively available for energy to be conducted away to the surrounding cooler substrate by thermal conduction. In this condition more energy is utilized for melting with a concomitant increase in the melting efficiency. A similar phenomenon applies to the effect of travel speed; the faster the heat source can travel while melting the substrate, the less time there is for heat to be conducted away from the locally heated region and the higher the melting efficiency.

These effects of arc power and travel speed on melting efficiency can be demonstrated with the aid of the analytical solution to the conduction heat flow

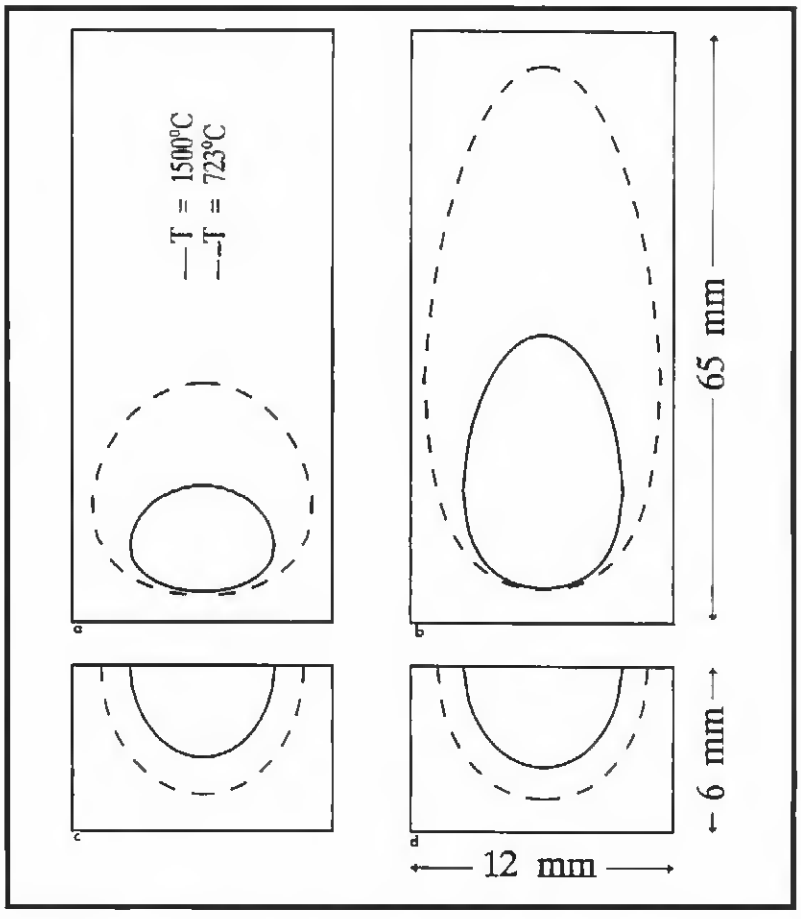

Fig. 12 — A and C — 1500° and 723°C isotherms for welding conditions of low arc power (3825 W) and travel speed (10 mm/s); B and D — high arc power (10,170 W) and travel speed (26 mm/s).

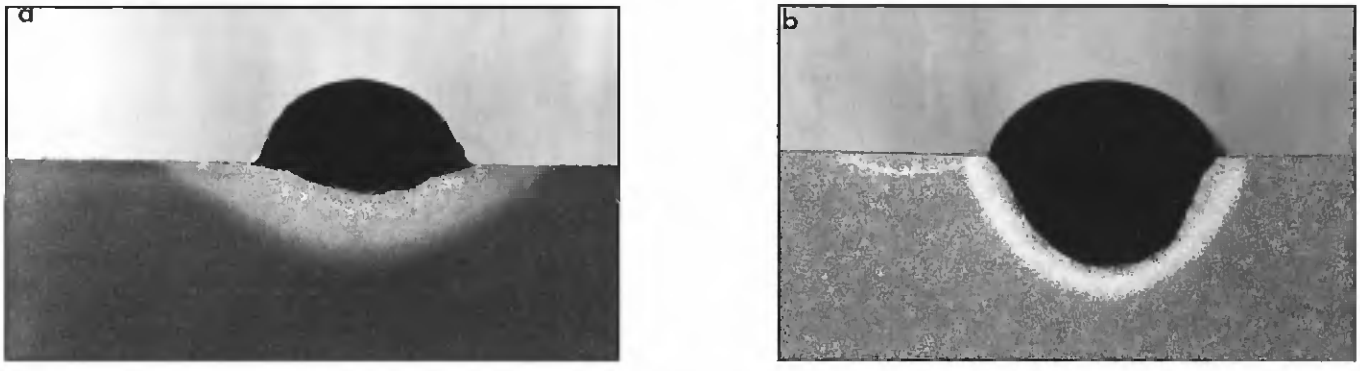

Fig. 13 — Cross-sectional photomacrographs of welds conducted under welding parameters shown in Fig. 12. A — arc power = 3825 W and travel speed = 10 mm/s; B — arc power = 10,170 W and travel speed = 26 mm/s.

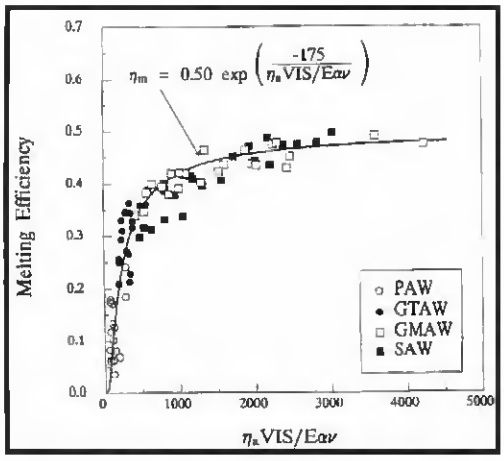

Fig. 14 — Melting efficiency of all the processes as a function of the dimensionless parameter $\eta_a VIS/E\alpha v$ with plot of semi-empirical relation.

equation derived hy Rosenthal (Ref. 21)

$$\frac{2\pi k(T-T_o)\,r}{\eta_a VI} = exp\frac{-S(r-x)}{2\alpha} \qquad (17)$$

Here, r is the radial distance from the heat source, x is the distance along the x axis (the direction of travel), and all other variables are as previously defined. Although this solution is derived based on a number of assumptions such as a point heat source, absence of melting, heat transfer by conduction only, and constant thermal properties, it is quite useful for examining the effect of welding parameters on melting efficiency. Because the solution was derived to describe thermal conduction in the base metal, it is valid to use this solution to describe the role of thermal conduction in melting efficiency as affected by the welding parameters.

Figure 12 shows the positions of the 1500°C (2732°F) (melting temperature) and 723°C (1333°F) (HAZ boundary) isotherms for two sets of welding conditions on steel as calculated by Equation 17. Figures 12A and B show the isotherms in the x-y plane, while Figs. 12C and D show the isotherms in the y-z plane. The y-z plane isotherms were taken at locations along the x axis where the 1500°C isotherms are widest and can be viewed as describing a weld in cross-section. The parameters used for each condition are listed in the figure. Note that the ratio of net arc power to travel speed (*i.e.*, net heat input/unit length of weld) is equivalent in each case. The corresponding experimental welds conducted under the same parameters are shown in Figs. 13A and B.

Comparison of Fig. 12A and C with 12B and D shows that increased arc power and travel speed moves the 1500°C isotherm out to a larger distance, which translates to a larger melt volume. Since the two conditions are conducted under equivalent net heat input, the melting efficiency is greater for the case of higher arc power and travel speed. In addition, the cross-sectional view shows that the distance between the melting point and HAZ boundary isotherms, which represents the size of the HAZ, decreases from 1.7 to 1.2 mm (0.07–0.05 in.) as the arc power and travel speed increase. Thus, in general, increases in arc power and travel speed move the high-temperature isotherms out to larger distances and decreases the distance between the individual isotherms, which leads to increased melting and a decreased HAZ size, a condition which is often highly desirable in industrial applications. These effects are readily observed in the experimental welds shown in Fig. 13. It should also be noted that, although each case was conducted under equivalent net heat input, the temperature distribution in each case is significantly different. This fact is rather important when considering heat flow simulation results which often state only the heat input/unit length of weld used for the calculations without regard for individual values of arc power and travel speed.

It should be noted that, in practical applications, the melting efficiency can not be increased indefinitely by an increase in travel speed when the arc power is held fixed. At some point, the travel speed will become too high for any melting to occur at all because there is insufficient time for energy transfer to the substrate. As a result, the melting efficiency can be expected to eventually drop to zero with a continuous increase in travel speed at a fixed arc power. To achieve a continuous increase in melting efficiency with travel speed, the arc power must be increased along with the travel speed to compensate for the decrease in time available for delivering energy to the substrate.

Melting Efficiency Processing Parameter Correlations

Fuerschbach and Knorovsky (Ref. 6) have demonstrated that melting efficiency can be predicted from the welding parameters and material properties by an equation of the form

$$\eta_m = A\ exp\left(\frac{-B}{\eta_a VIS\ /\ E\alpha v}\right) \qquad (18)$$

Here, E is used to represent the total enthalpy change due to melting, α is the thermal diffusivity at 300 K, and v is the kinematic viscosity at the melting point. Thus, the quantity $(\eta_a VIS/E\alpha v)$ is a dimensionless parameter, analogous to that of $(8\alpha/5Sd)$ in Equation 16. The constant A is representative of the maximum melting efficiency for a given joint or substrate geometry, which is obtained when the quantity $(\eta_a VIS/E\alpha v)$ is large. The constants A and B can be determined from the intercept (A) and slope (B) on a plot of ln (η_m) against $(\eta_a VIS/E\alpha v)^{-1}$. Figure 14 shows melting efficiency plotted against this dimensionless parameter. An average value between carbon steel and austenitic stainless steel of E = 9.6 Jmm^{-3} and v = 0.84 mm^2s^{-1} was used. The effect of thermal diffusivity should be controlled by the substrate, so the value for steel was used (9.1 mm^2s^{-1}, Ref. 2). With these values $E\alpha v = 73\ J \cdot mm \cdot s^{-2}$. Since the substrate and filler metal are held constant in this experiment and the value of Eαv is therefore fixed, the replot of the data using this dimensionless parameter does not provide an opportunity to reveal its effectiveness to normalize the influence of material property variations. However, this parameter has been shown to normalize differences between 304 stainless steel and NI 200 in an edge weld configuration (Ref. 6). Therefore, the approach is adopted here for comparisons to possible future results. Equation 18 is plotted in Fig. 14 with the constants A = 0.50 and B = 175, and the expression provides a good representation of the experimental data. The use of this dimensionless parameter warrants further considerations with various materials and geometries as it provides a method for predicting parameters that optimize melting efficiency.

Arc Efficiency-Melting Efficiency Interactions

As shown by inspection of Figs. 3 and 11, a low arc efficiency appears to limit the maximum achievable melting efficiency. When the arc efficiency is low, energy cannot be transferred to the substrate at high rates, and it is difficult to reach high melting efficiencies. The arc efficiency also affects the melting efficiency by limiting the maximum travel speed which can be obtained. As noted earlier, operation at fast travel speeds requires high arc powers to compensate for the decreased time available for energy transfer to the substrate by the heat source. If the maximum deliverable arc power is limited due to a low arc efficiency, then the maximum travel speed will also be limited and produce a further

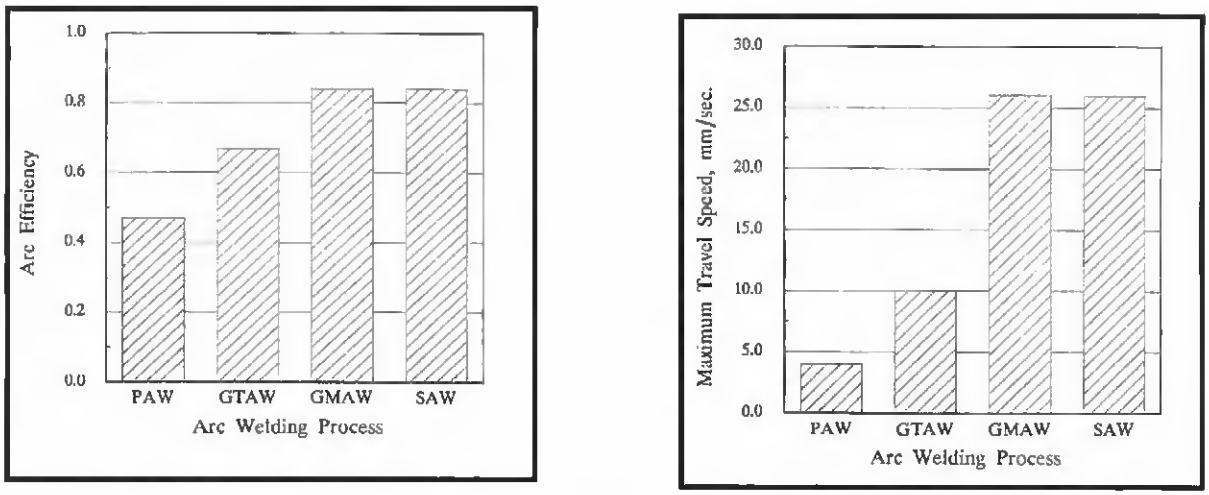

Fig. 15 — A — Comparison of arc efficiencies; B — maximum achievable travel speeds among the processes evaluated.

reduction in the melting efficiency. This trend is revealed for the present set of conditions in Fig. 15 where the arc efficiencies and maximum travel speeds for the processes are compared. Note that the maximum travel speed scales directly with the arc efficiency. For the consumable electrode processes, the arc efficiency is high ($\eta_a = 0.84$), which permits a high rate of net energy transport to the substrate and the achievement of high travel speeds. As the arc efficiency decreases for the nonconsumable electrode processes, the net power delivered to the substrate is reduced and causes a concomitant reduction in the maximum travel speed that can be achieved. The results of these effects on the maximum achievable melting efficiency are shown in Fig. 16, where it is readily observed that the maximum melting efficiency scales directly with the arc efficiency and maximum travel speed.

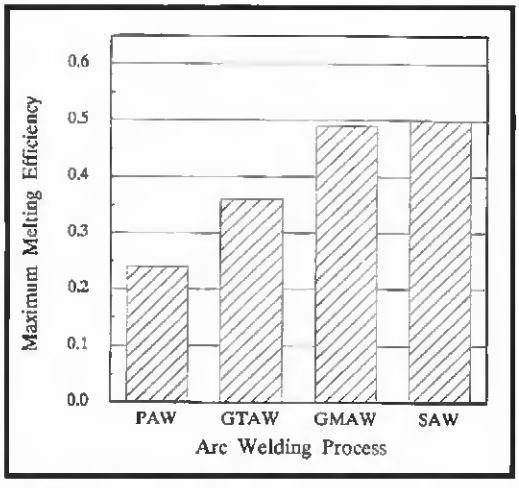

Fig. 16 — Comparison of maximum melting efficiencies achieved with each process. The maximum melting efficiency scales directly with the arc efficiency and maximum travel speed of each process.

As a final comment, it is useful to compare the melting efficiency achieved with the consumable electrode arc welding processes studied here with values typically reported for the high-energy-density processes such as laser and electron beam. The high-energy-density processes are often selected for surfacing (and other) applications due to their ability to produce welds with minimal heat-affected zones. In other words, they can operate at high melting efficiencies. However, the theoretical maximum melting efficiency is 0.48, which is in very good agreement with the experimentally measured maximum determined by a number of investigators, including the laser and electron beam processes (Ref. 20). Therefore, as recently pointed out (Ref. 6), once a melting efficiency of approximately 0.48 is reached, no further increase is possible, regardless of the process being used. Figure 12 clearly shows that the consumable electrode processes are capable of achieving this optimum condition for the present set of conditions when the welding parameters are carefully selected. Therefore, the advantage of high melting efficiency exhibited by the high-energy-density processes can be achieved with the relatively inexpensive and easily operated consumable electrode arc processes when the parameters are carefully optimized.

Conclusions

A study has been conducted on the arc and melting efficiency of the PAW, GTAW, GMAW, and SAW processes. The following conclusions can be drawn from this work:

1) The arc efficiency did not vary significantly within a given process over the range of currents investigated. The following values were measured: PAW — $\eta_a = 0.47 \pm 0.03$, GTAW — $\eta_a = 0.67 \pm 0.05$, and GMAW and SAW — $\eta_a = 0.84 \pm 0.04$.

2) The I^2R power of the GMAW consumable electrode was calculated to account for 14 to 18% of the total power supplied to the workpiece and was used to account for observed differences in arc efficiency between the GMAW and GTAW processes. The super-heated liquid drops were calculated to account for 38 to 42% of the total power supplied to the workpiece, which is in good agreement with experimentally measured values.

3) The melting efficiency can be estimated for the present set of conditions from the semi-empirical relation

$$\eta_m = 0.50 \ exp\left(\frac{-175}{\eta_a VIS \ / E\alpha v}\right)$$

4) There is an interaction between the arc and melting efficiency. A low arc efficiency will limit the power delivered to the substrate which, in turn, limits the maximum travel speed for a given set of conditions. As a result, a low arc efficiency can limit the maximum obtainable melting efficiency.

Acknowledgments

The authors gratefully acknowledge the support of this work by Ohio Edison, Potomac Electric Power Company, Pennsylvania Electric Energy Research Council, Dayton Power & Light, Public Service

Electric & Gas, and Virginia Power. The assistance in metallographic preparation by A. O. Benscoter, review of heat flow considerations by Mark D'Agostini, and design and construction of the welding laboratory by L. R. Clements are also appreciated.

References

1. Niles, R. W., and Jackson, C. E. 1975. Welding thermal efficiency of the GTAW process. *Welding Journal* 54 (1): 25-s to 32-s.

2. Kou, S. 1987. *Welding Metallurgy*. New York, N.Y., Wiley.

3. Lancaster, J. F., ed. *The Physics of Welding*. Oxford, England, Pergamon Press.

4. Wells, A. A. 1952. Heat flow in welding. *Welding Journal* 31 (5): 263-s to 267-s.

5. Okada, A. 1977. Applications of melting efficiency and its problems, *Journal of the Japan Welding Society*, 46 (2): 53 to 61.

6. Fuerschbach, P. W. and Knorovsky, G. A. 1991. A study of melting efficiency in plasma arc and gas tungsten arc welding. *Welding Journal* 70 (11): 287-s to 297-s.

7. DuPont, J. N. and Marder, A. R. 1995. Dilution in single pass arc welds, submitted to *Metallurgical Transactions*.

8. Geidt, W. H., Tallerico, L. N., and Fuerschbach, P. W. 1989. GTA welding efficiency: calorimetric and temperature field measurements. *Welding Journal* 68 (1): 28-s to 32-s.

9. Quigley, M. B. C., Richards, P. H., Swift-Hook, D. T., and Gick, A. E. F. 1973. Heat flow to the work piece from a TIG welding arc. *J. Phys. D: Appl. Phys.* 6: 2250– 2258.

10. Glickstein, S. S. 1982. Basic studies of the arc welding process. *Proc. Trends in Welding Research in the United States*. ed. S. A. David, pp. 3–50, ASM International, Materials Park, Ohio.

11. Smartt, H. B., Stewart, J. A., and Einerson, C. J. 1985. Heat transfer in gas tungsten arc welding. *Proc. ASM Intl. Welding Congress*, ASM 8511-011.

12. Apps, R. L., and Milner, D. R. 1955. Heat flow in argon arc welding. *British Welding Journal* 2 (10): 475–485.

13. Watkins, A. D., Smartt, H. B., and Einerson, C. J. 1990. Heat transfer in gas metal arc welding. *Proc. Recent Trends in Welding Science and Technology*, eds. S. A. David and J. M. Vitek, pp., 19–23, ASM International, Materials Park, Ohio.

14. Feith, A. D., Hein, C. P., Johnstone, C. P., and Flagela, P. N. 1968. Thermophysical properties of low carbon 304 stainless steel to 1350°C. EMP 643.

15. Fine, H. A., and Geiger, G. H. 1979. *Handbook on Material and Energy Balance Calculations in Metallurgical Processes*, AIME, Warrendale, Pa.

16. Lucks, C. F., and Deem, H. W. 1958. Thermal properties of thirteen metals. STP No. 227, ASTM, Philadelphia, Pa.

17. Kou, S., and Tsai, M. C. 1985. Thermal analysis of GTA welding electrodes. *Welding Journal* 64 (9): 266-s to 269-s.

18. Wasznik, J. H., and Van Den Heuvel, J. P. M. 1982. Heat generation and heat flow in the filler metal in GMA welding. *Welding Journal* 61 (8): 269-s to 282-s.

19. Metcalfe, J. C., and Quigley, B. C. 1975. Heat transfer in plasma-arc welding. *Welding Journal* 54 (3): 99-s to 103-s.

20. Arata, Y. 1986. *Plasma, Electron & Laser Beam Technology*, ASM International, Materials Park, Ohio.

21. Rosenthal, D. 1946. The theory of moving sources of heat and its application to metal treatments. *Trans. of the ASME*, 68: 849 to 866.

22. Geiger, G. H. and Poirier, D. R. 1973. *Transport Phenomena in Metallurgy*. Addison-Wesley Publishing Company, Reading, Mass.